A Confocal Microwave Imaging Algorithm for Breast Cancer Detection

Xu Li, *Student Member, IEEE,* and Susan C. Hagness, *Member, IEEE*

***Abstract*—We present a computationally efficient and robust image reconstruction algorithm for breast cancer detection using an ultrawideband confocal microwave imaging system. To test the efficacy of this approach, we have developed a two-dimensional (2-D) anatomically realistic MRI-derived FDTD model of the cancerous breast. The image reconstruction algorithm is applied to FDTD-computed backscatter signals, resulting in a microwave image that clearly identifies the presence and location of the malignant lesion. These simulations demonstrate the feasibility of detecting and imaging small breast tumors using this novel approach.**

***Index Terms*—Breast cancer detection, FDTD, microwave imaging, ultrawideband radar.**

I. Introduction

X-RAY mammography is the most effective imaging method for detecting nonpalpable early-stage breast cancer. However, despite significant progress in improving mammographic technique, persisting limitations result in relatively high false negative and false positive rates, particularly in pre-menopausal women where increased breast density can obscure nonpalpable lesions. Therefore, techniques that image other physical tissue properties are under investigation. The significant contrast in the dielectric properties of normal breast tissue and malignant tumors [1]–[3] provides a strong rationale for nonionizing microwave breast imaging. Narrowband microwave tomography [4], [5] recovers the dielectric properties in the reconstructed image, but requires computationally intensive algorithms to solve the inverse scattering problem. In this paper, we show that pulsed confocal microwave imaging (CMI) [6], [7] permits simpler, yet robust image reconstruction for detecting breast cancer.

In our approach, each element of an antenna array sequentially transmits an ultrashort pulse into the breast and collects the backscatter signal. The backscatter waveforms at all antennas are then time-shifted and added to create a synthetic focal point. The position of the focus is scanned throughout the breast by adjusting the distribution of time shifts of the stored backscatter waveforms for each new focal point. If a high-contrast scattering object, such as a malignant tumor, exists at the focal point, the waveforms add coherently. Clutter signals generated by the heterogeneity of normal breast tissue surrounding the focal point will add incoherently. In this manner, tumor backscatter signals are enhanced while clutter signals are minimized. Systematic scanning of the synthetic focus from point to point within the breast creates a microwave image of significant scattering points within the breast.

Manuscript received July 26, 2000; revised December 6, 2000. This work was supported by The Whitaker Foundation Biomedical Engineering Research Grant RG-99-0004. Computing resources were provided in part by Cray, Inc.

The authors are with the Department of Electrical and Computer Engineering, University of Wisconsin, Madison, WI 53706 USA (e-mail: hagness@engr.wisc.edu).

Digital Object Identifier S 1531-1309(01)03213-5

II. System Configuration and Modeling

We consider a system configuration where an antenna array is placed at the surface of the naturally flattened breast of a patient lying in a supine position. An important feature of this chosen orientation is the ability to access the upper outer quadrant of the breast where almost 50% of cancers occur [8]. This region is difficult to access when the breast is compressed, as is the case with X-ray mammography, or extends through an opening in the scan table, as is the case with microwave tomography [5] and an alternative CMI configuration [9].

To test the image reconstruction algorithm presented in Section III, we developed a realistic FDTD model of the naturally flattened breast. For these feasibility studies, we present a two-dimensional (2-D) model; however, the work presented here is directly applicable to the three-dimensional (3-D) case. A high-resolution breast MRI data set was obtained during a scan of a patient lying in a prone position. A low-resolution scan was taken with the same patient in a supine position. Using the low-resolution face-up MRI data set as a guide, we vertically compressed and laterally expanded the high-resolution face-down images so that the overall shape of the breast matched that of the naturally flattened breast in the face-up position. We segmented the skin layer and removed the subtle MRI artifacts adjacent to the skin. Finally, we used a linear interpolation scheme to change the MRI pixel size (0.625×0.625 mm^2) to the desired FDTD grid cell size (0.5×0.5 mm^2). The resulting FDTD grid is terminated with PML absorbing boundary conditions (see Ch. 7 in [10]).

The frequency dependence of the dielectric constant, ϵ_r, and conductivity (S/m), σ, has been incorporated into the FDTD model using an auxiliary differential equation formulation (see Ch. 9 in [10]) for a first-order (Debye) dispersion:

$$\epsilon_r - j\frac{\sigma}{\omega\epsilon_0} = \epsilon_\infty + \frac{\epsilon_s - \epsilon_\infty}{1 + j\omega\tau} - j\frac{\sigma_s}{\omega\epsilon_0} \tag{1}$$

As shown in Fig. 1, the Debye parameters have been chosen to fit the published data for normal ($\epsilon_s = 10$, $\epsilon_\infty = 7$, $\sigma_s = 0.15$ S/m, $\tau = 6.4$ ps) and malignant ($\epsilon_s = 50$, $\epsilon_\infty = 4$, $\sigma_s = 0.7$ S/m, $\tau = 6.4$ ps) breast tissue up to 3 GHz. For reference, the shaded region of Fig. 1 marks the 3-dB bandwidth of the pulse used in Section III.

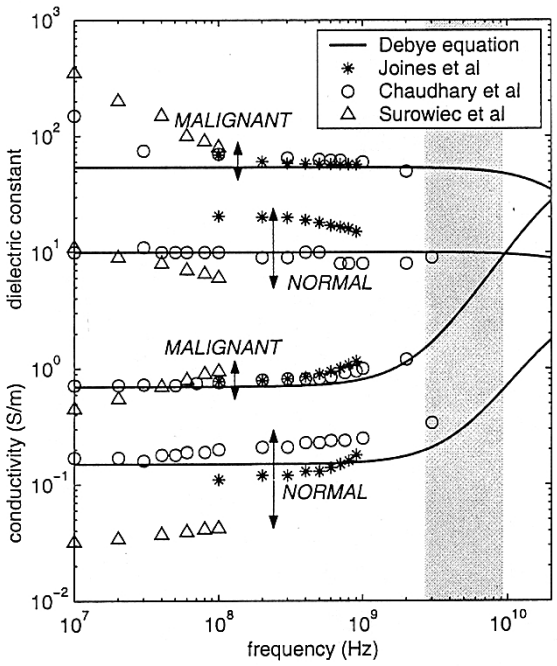

Fig. 1. Single-pole Debye curve fits of measured baseline dielectric-properties data for normal and malignant breast tissue at radio and microwave frequencies.

Fig. 2 shows the spatial variation of the dielectric properties at 6 GHz. To preserve the heterogeneity of normal breast tissue, we linearly mapped the range of MRI pixel densities in the breast interior to a range of Debye parameters representing a variation of $\pm 10\%$ around an estimated baseline ($\epsilon_{r,\mathrm{avg}} = 9.8$, $\sigma_{\mathrm{avg}} = 0.4$ S/m at 6 GHz). This variation represents an upper bound on reported breast tissue variability [6], which presumably covers the range from fat to fibroglandular tissue. Thus, regions of dense fibroglandular tissue were assigned Debye parameters yielding the largest values of ϵ_r and σ. Similarly, regions of fatty tissue were assigned the smallest values. In the model shown in Fig. 2, a 2-mm-diameter malignant tumor ($\epsilon_r = 50.0$, $\sigma = 7.0$ S/m at 6 GHz) has been artificially introduced at a depth of 3.1 cm below the surface of the 2-mm-thick skin layer ($\epsilon_r = 36$, $\sigma = 4$ S/m at 6 GHz [6]).

III. Image Reconstruction Algorithm

In our FDTD simulations, an antenna array consisting of $M = 17$ monopoles spanning 8 cm is placed along the surface of the breast. The array is backed with a low-loss dielectric material matching the nominal dielectric properties of the breast. A simulated scan involves exciting each antenna individually with a short pulse and collecting the backscatter response at the same antenna element. This process is repeated for each element of the array, resulting in M received backscatter waveforms.

These stored waveforms include the incident signal and skin backscatter, both of which appear early on and at the same point in time in each of the waveforms. Since we want to image neither the incident signal nor the skin, these artifacts are removed using a robust calibration process that avoids the use of a breast phantom or *a priori* information.

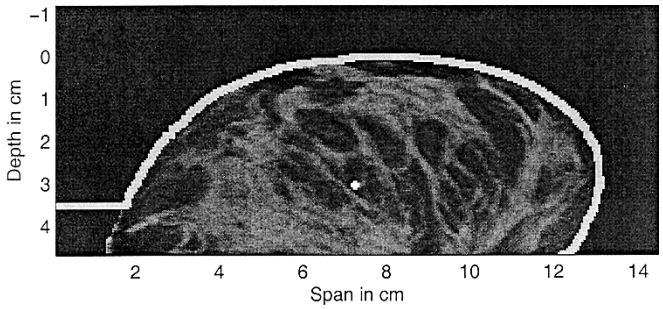

Fig. 2. Two-dimensional dielectric-properties breast model derived from an MRI scan. A 2-mm-diameter malignant tumor has been inserted at a depth of 3.1 cm.

A reference waveform is simply created by averaging the M stored waveforms. The skin backscatter and incident signals remain dominant in this reference waveform while the tumor backscatter and clutter signals are reduced to negligible levels. The reference waveform is then subtracted from each of the M original backscatter waveforms, resulting in M calibrated backscatter waveforms that essentially contain only the tumor response and clutter signals. As a final step in the calibration proess, low-frequency signal content is removed by subtracting from each waveform its moving average.

The calibrated data set is in the form of M vectors: A_1, A_2, …, A_M, with each vector containing N time-sampling points. The following algorithm describes the coherent-sum process adapted from synthetic aperture radar techniques. The mth discrete-time delay needed to achieve a synthetic focus of the M backscatter waveforms at position vector $\vec{r}$ in the breast is given by $\tau_m(\vec{r}) = 2d_m(\vec{r})/(v\Delta t)$, where $d_m(\vec{r}) = |\vec{r} - \vec{r_m}|$ is the distance between the synthetic focal point and the mth transmit/receive antenna element located at position $\vec{r_m}$, v is the average velocity of propagation in the breast at the center frequency of the pulse (approximately 6 GHz), and Δt is the time-sampling interval between data points. In our 2-D example, $\vec{r} = (x, y)$; in 3-D space, $\vec{r} = (x, y, z)$.

The ultrawideband waveform used in our simulation is a differentiated Gaussian pulse with a temporal duration of 110 ps (full-width half-maximum). Because of the pulse's zero-crossing, $A_m(\tau_m(\vec{r})) \approx 0$ for a synthetic focal point location coinciding with the coordinates of a scattering object. To obtain a nonzero sum in the subsequent step, each calibrated backscatter waveform is integrated over time to obtain M vectors: B_1, B_2, …, B_M.

The reconstructed image is created by time-shifting and summing data points from each calibrated, integrated waveform for each synthetic focal point in the breast. The intensity of a pixel in the reconstructed image sum for a specific synthetic focal point is assigned the square of the coherently summed values:

$$I(\vec{r}) = \left[\sum_{m=1}^{M} w_m B_m(\tau_m(\vec{r}))\right]^2 \tag{2}$$

where the weights w_m are introduced to compensate for the radial spreading of each cylindrical wave as it propagates outward from the transmitting antenna.

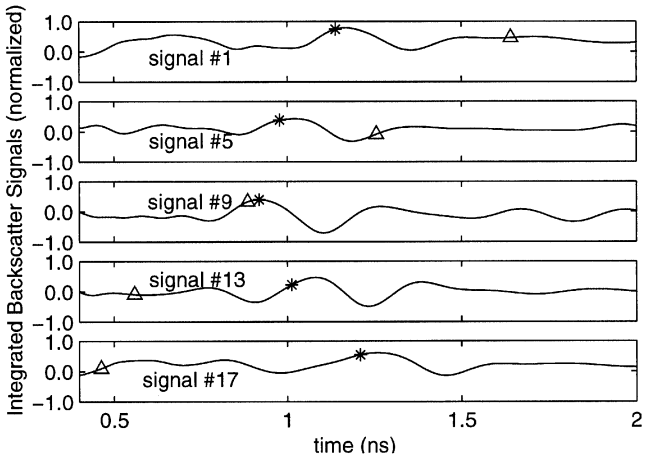

Fig. 3. Processed backscatter waveforms computed for an MRI-derived breast model containing a 6-mm-diameter tumor at a depth of 3.3 cm. The asterisks (∗) mark the time delays corresponding to a synthetic focal point located within the tumor; the triangles (△) mark the time delays corresponding to a focal point away from the tumor.

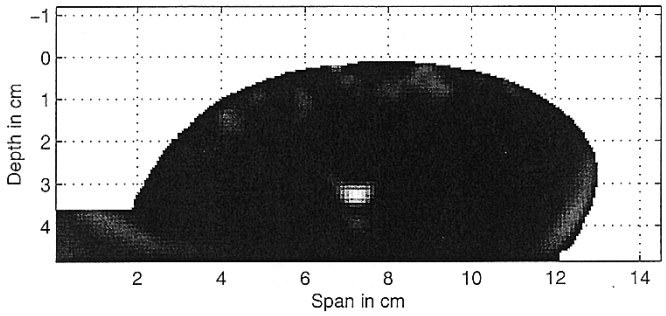

Fig. 4. Two-dimensional microwave breast image reconstructed from the processed backscatter waveforms computed for the model of Fig. 2.

IV. Numerical Results and Discussion

The coherent-addition process described by (2) is illustrated in Fig. 3, which shows a subset of calibrated, integrated backscatter waveforms computed from an FDTD model containing a 6-mm-diameter malignant tumor at a depth of 3.3 cm. Two sets of time delays are marked on the backscatter waveforms. The set of asterisks show the time delays estimated for a synthetic focal point located within the region of the tumor. These marked field values will add coherently. The other set of time delays corresponds to a synthetic focal point located 3 cm to the right of the tumor, at a depth of 1.3 cm. Those marked field values will add incoherently.

The synthetic focal point is scanned throughout the breast in increments of 1mm^2. Each value of I is converted to a grayscale pixel using an appropriate mapping function. The reconstructed microwave image is shown in Fig. 4. The bright spot located at a depth of approximately 3 cm is at precisely the location of the 2-mm-diameter malignant tumor present in the FDTD model. The image also shows the strong suppression of clutter signals generated by the tissue heterogeneity in the surrounding regions. The visible clutter near the surface of the breast represents remnants of incident signal and skin backscatter that remain after the calibration process. These artifacts can be further reduced by increasing the number of antennas used in the array.

We have estimated the signal-to-clutter (S/C) ratio, defined as the ratio of the tumor-response peak to the maximum clutter response in the breast interior (at depths of 1 cm or more below the skin surface), to be approximately 8 dB for the breast model containing the 2-mm-diameter tumor. We also calculated the lateral full-width of the tumor response at the half-maximum to be on the order of 5 mm. Performance of this system in 3-D will, of course, depend on the number and type of antenna elements and the dimensions of the 2-D array. Based on our preliminary experience with 3-D breast models, we expect to be able to obtain comparable or even superior performance in 3-D.

FDTD simulations have demonstrated that computationally efficient signal processing techniques can be applied to microwave backscatter data in a straightforward manner that avoids solving the inverse scattering problem. The signal processing techniques employed in CMI are robust with respect to uncertainties in the time delays required for the coherent-addition process, and therefore do not appear to be hindered by the heterogeneous and dispersive nature of the breast.

Acknowledgment

The authors wish to thank Dr. F. Kelcz for providing the breast MRI data, Dr. C. Furse for helpful discussions on creating MRI-derived FDTD models, and Ms. E. Fear and Dr. M. Stuchly for their support of CMI.

References

[1] W. T. Joines, Y. Z. Dhenxing, and R. L. Jirtle, "The measured electrical properties of normal and malignant human tissues from 50 to 900 MHz," *Med. Phys.*, vol. 21, pp. 547–550, Apr. 1994.

[2] S. S. Chaudhary, R. K. Mishra, A. Swarup, and J. M. Thomas, "Dielectric properties of normal and malignant human breast tissues at radiowave and microwave frequencies," *Indian J. Biochem. Biophys.*, vol. 21, pp. 76–79, Feb. 1984.

[3] A. J. Surowiec, S. S. Stuchly, J. R. Barr, and A. Swarup, "Dielectric properties of breast carcinoma and the surrounding tissues," *IEEE Trans. Biomed. Eng.*, vol. 35, pp. 257–263, Apr. 1988.

[4] A. E. Souvorov, A. E. Bulyshev, S. Y. Semenov, R. H. Svenson, and G. P. Tatsis, "Two-dimensional computer analysis of a microwave flat antenna array for breast cancer tomography," *IEEE Trans. Microwave Theory Tech.*, vol. 48, pp. 1413–1415, Aug. 2000.

[5] P. M. Meaney and K. D. Paulsen, "Nonactive antenna compensation for fixed-array microwave imaging—Part II: Imaging results," *IEEE Trans. Med. Imag.*, vol. 18, pp. 508–518, June 1999.

[6] S. C. Hagness, A. Taflove, and J. E. Bridges, "Two-dimensional FDTD analysis of a pulsed microwave confocal system for breast cancer detection: Fixed-focus and antenna-array sensors," *IEEE Trans. Biomed. Eng.*, vol. 45, pp. 1470–1479, Dec. 1998.

[7] ——, "Three-dimensional FDTD analysis of a pulsed microwave confocal system for breast cancer detection: Design of an antenna-array element," *IEEE Trans. Antennas Propagat.*, vol. 47, pp. 783–791, May 1999.

[8] W. H. Parsons, *Cancer of the Breast*. Springfield, IL: Charles Thomas, 1959.

[9] E. C. Fear and M. A. Stuchly, "Microwave system for breast tumor detection," *IEEE Microwave Guided Wave Lett.*, vol. 9, pp. 470–472, Nov. 1999.

[10] A. Taflove and S. C. Hagness, *Computational Electrodynamics: The Finite-Difference Time-Domain Method*, 2nd ed. Boston, MA: Artech House, 2000.